Low-Thrust Orbital Maneuver Analysis for Cubesat Spacecraft with a Micro-Cathode Arc Thruster Subsystem

IEPC-2013-365

Presented at the 33rd International Electric Propulsion Conference,
The George Washington University • Washington, D.C. • USA
October 6 – 10, 2013

Samudra E. Haque[1], Michael Keidar[2] and Taeyoung Lee[3],
The George Washington University, Washington, DC 20052, USA

Abstract: Micro-cathode arc thruster has been proposed for small spacecraft micropropulsion. The technology has several desirable properties for applications in Space, such as high specific impulse, low energy consumption, and low input voltage range. In particular, it has a compact and simple concentric design with no moving parts for extremely high reliability, and it yields extended operation lifetime. In this paper, analytical studies are presented to demonstrate its effectiveness for various basic and necessary CubeSat class spacecraft maneuvers. Analyzing the effects of low-thrust is challenging, as small variations of orbital properties should be accurately computed over a long-time period. We present simplified orbital analysis based on the secular change of orbital elements derived from orbital perturbation theory. It is shown that micro-cathode thruster can be effectively used for each phase of a CubeSat mission, including orbital regularization, and inclination changes. This paper presents a first comprehensive model/simulation for a quick analysis for the capabilities of micro-cathode thruster in orbital maneuvering for CubeSats.

Nomenclature

Isp	=	Specific Impulse (seconds)
J-SSOD	=	Japan Experiment Module – Kibo Exposed Facility – Small Satellite Orbital Deployer
P-POD	=	Poly-PicoSatellite Orbital Deployer
TH	=	Thruster Head
PPU	=	Plasma Power Unit

I. Introduction

The Micro-propulsion and Nanotechnology Laboratory (MpNL), of the Dept. of Mechanical and Aerospace Engineering at The George Washington University, has been conducting fundamental and applied research[1-11], since 2007, in order to develop a scalable and modular, "In-Space Propulsion" subsystem, utilizing the novel plasma micro-propulsion technology called Micro-Cathode Arc Thruster (μCAT). This system is meant for applications in small spacecraft, of various sizes, ranging from Nano-satellites (1-10 Kg) to Mini-satellites (100 Kg or higher). The principal means of propulsion is the application of moderate direct current, in very brief interval pulses, with a high initial peak voltage of miniscule duration, to a concentric pair of anode, cathode terminals. The cathode material is ablated in miniscule quantities, by the very energetic, but minute, vacuum arc discharge. The evaporated material in the form of quasi-neutral plasma comprises the exhaust of the thruster. Micro-cathode arc thrusters have several desirable properties for micro-propulsion applications in space, such as high

[1] Ph.D Student, Dept. of Mech. and Aerospace Engineering, samudra@gwu.edu
[2] Professor of Engineering and Applied Science, Dept. of Mech. and Aerospace Engineering, keidar@gwu.edu
[3] Assistant Professor of Engineering and Applied Science, tylee@gwu.edu

specific impulse, low energy consumption, and low input voltage range. In particular, it has a compact and simple concentric deign with no moving parts for extremely high reliability, and it yields extended operation lifetime that is suitable for space missions.

A. Ongoing μCAT research and development

Since 2007 several types of μCAT-based thruster heads, and thruster power/plasma processing units (PPU) have been produced at the MpNL with various operational characteristics (e.g., different Isp, different operating voltages, different mass, different performance levels, etc.). All components have been designed with the potential of being able to be used in small spacecraft with different bus architectures and mass sizes. Some of the different thruster head models are:

- Ring Electrode (RE) – Anode/Cathode terminals are placed end to end, separated by a thin insulating ring,
- Coaxial Electrode (CE, a.k.a. Gen. II/G2) – Concentric Anode/Cathode terminals
- Alternating Electrode (AE) – Dual cathode terminals, with a single Anode terminal
- Bi-Modal (BM) – Similar to Gen II/G2, but reversible terminals

A generic μCAT channel consists of:

- Thruster head (TH)
- Optional electromagnet (EM)
- Plasma processing unit (PPU), also known as, "power processing unit"

Several μCAT channels can be combined into a "subsystem" with a common Power Management (PM) section, Control Unit (CU) section and optionally varying configurations of Thruster Head arrangements (e.g., array, cluster, hybrid cluster-array)[5, 12].

Per experimental results obtained in 2010/2011[7], an average impulse-bit produced by a μCAT channel being triggered at *F=50 Hz* rate, by an external control device, has been characterized and measured to be 1.15 *uN*. In 2013, recently developed MpNL PPU hardware was used in demonstrations at NASA Ames Research Center (ARC) of a 3-channel μCAT subsystem[12], as part of the Micro-Cathode Arc Thruster PhoneSat Experiment (MCATPE), with programmable frequencies of *F=1 Hz* to *F=10 Hz,*. Hardware redesign is underway to accommodate fully programmable thruster channel operation up to *F=50 Hz* with appropriate sensor telemetry feedback. Analyzing the effects of such continuous low-thrust impulse-bits is challenging, as small variations of orbital properties need to be accurately computed over a long-time period.

B. Cubesat class spacecraft

CubeSats are a class of multi-purpose nanosatellites[13], that are based upon the principle of a common orbital deployer (e.g., a P-POD), and a lightweight bus comprised of stackable 3-D rectangular frame. The volume of each nominal cell, or "U", is typically 1000 cm^3 with total external dimensions of the bus being limited to 10 cm in two axes, and a third axes allowed to be up to 30 cm in length. Since the first successful launch in 2003, the CubeSat specifications[4], under development since 1999 jointly by California Polytechnic State University and Stanford University, have been standardized for space science and exploration of small satellites, especially from academia. At present, the total mass of each "U", or frame, has to be constrained to typ. 1.33 Kg. Several recent CubeSat missions and related projects include biological science microsatellites, PharmaSat[14, 15], O/OREOS[16] (with participation by GWU faculty), PhoneSat[17-25], and numerous other missions sent to space under the NASA Educational Launch of Nanosatellites (ELaNA) program[26-28].

C. Objective

In this paper, we wish to present preliminary analysis to show that a μCAT subsystem is an effective micro-propulsion device for CubeSat systems, by modeling various necessary, and basic, orbital maneuvers using pulsed sequences of low-thrust.

We present simplified orbital analysis based on the secular change of orbital elements derived from orbital perturbation theory[29-31]. Key phases of a hypothetical CubeSat mission will be investigated: (a) overcoming drag in LEO (b) deployment from the J-SSOD unit on the ISS and separation (c) initial orbit (d) orbit circularization (e) inclination correction of eccentricity. The main contribution of this paper is to establish a working model/simulation that can be used to generate thorough and comprehensive analysis of the capabilities of μCAT subsystem applications in orbital maneuvering for CubeSats.

[4] See Cubesat Design Specification, Rev. 12. http://www.cubesat.org/images/developers/cds_rev12.pdf

II. Theory and Model

A. Scalable Thrust Models

Different mechanical/electrical configurations of the components of a µCAT subsystem have been proposed by Haque for increasing thrust output levels (by varying the number of operational channels, operating frequency), or for producing precision levels of thrust (using hybrid approach), and for developing redundancy (clustering and arraying).

1. Single Channel

A single PPU (e.g. PPU/1) is used to power a single TH (TH/A), triggered by a single control signal (TP/1). This is a stand-alone configuration and is likely the simplest implementation method.

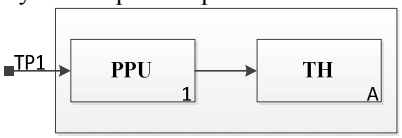

Figure 1 Single Channel

2. µCAT Array

A collection of PPU units (e.g. PPU/2-4), each with its own TH, as a single channel. Each channel can be triggered individually, or as a group. This configuration was chosen for MCATPE, with all trigger pulses inputs being fed by the same signal.

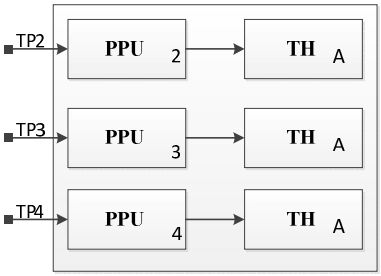

Figure 2 Array

3. µCAT Cluster

In a future configuration, certain in-space applications may call for expanded thruster capability, or potentially a switching method where some of the thrusters are activated, while others are not, from the same PPU. Examples of the later case may be opposing thrusters that are placed in a parallel direction, creating a 1-axis control mechanism.

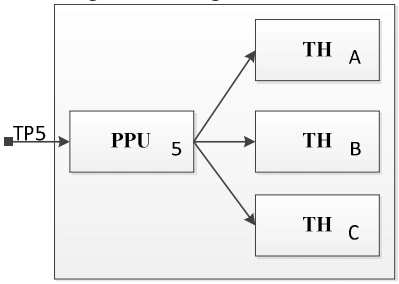

Figure 3 Cluster (w/optional Switch)

4. µCAT Cluster-Array Hybrid

If a larger spacecraft bus is available, arrays of µCAT devices (e.g., PPU/6) could potentially be combined with Cluster (e.g. PPU/7). This configuration is most suitable for varying power levels. Triggers could be all the same, but could also be manipulated to be independent from each other.

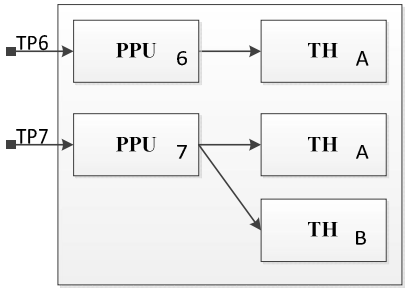

Figure 4 Hybrid Cluster/Array

As an example, three similar μCAT channels, of an Array, firing in a synchronized manner, at *F=1 Hz*, would be expected to produce three times the nominal thrust of a single channel. Alternatively a single μCAT channel could be pulsed at *F=3 Hz* to produce a force equal to the combined output of the three channels, so the effective thrust range of such a three-channel (1 Hz min, 50 Hz max) subsystem would be ~1 μN to ~0.173 mN.

B. Initial Orbit of ISS

Small spacecraft of CubeSat size and form factor typically do not warrant the expense required to have a dedicated launch to Space. The most accepted method of being sent aloft from Earth, is to be included as a secondary payload on any launch vehicle, to be deployed in Space from a CubeSat deployer. A convenient alternative exists for selected CubeSat missions, the spacecraft can now be packaged as cargo bound for the International Space Station (ISS), to be unpacked and setup by astronauts, who will then deploy the spacecraft using JAXA[5] Japanese Experiment Module (JEM) Small Satellite Orbital Deployer[32-34] (J-SSOD). This mechanism deploys clusters of CubeSats, at a separation velocity of 1.1-1.7 m/s, with a deploy direction angle of 45 degrees from nadir to aft axis, in a cone with a half angle of 18 deg. In terms of modeling constraints, it is similar to the deployment (e.g., ejection) process of a small spacecraft from an launch vehicle, or mothership, as can be seen in Figure 5.

Figure 5 On-orbit deployment scenarios (A) ISS (B) Launch Vehicle

[5] Japan Aerospace Exploration Agency, http://www.jaxa.jp

C. Atmospheric Drag

Once on-orbit as a stand-alone spacecraft, it is assumed that the drag coefficient C_D = 2.2 for our hypothetical spacecraft. For 1U CubeSats with the size of 1000 cm^3, the surface area projected onto the plane normal to the velocity vector is A = 100 cm^2, when its attitude is stabilized. The corresponding ballistic coefficient B is given by

$$B = \frac{C_D A}{m} = 0.088 \frac{m^2}{kg} \tag{1}$$

The deceleration due to atmospheric drag is given by

$$d = \frac{1}{2}\rho v_r^2 \left(\frac{C_D A}{m}\right) = \frac{1}{2}\rho v_r^2 B \tag{2}$$

where ρ is the density of atmosphere, and v_r is the relative velocity of the satellite with respect to the atmosphere. The atmospheric density at a specific altitude varies according to several factors such as solar activity. The atmospheric density, computed from the MSIS90E model is shown at FIGURE XX for three levels of solar activities[35]. Assuming that the atmosphere is rotating at the same rate of the Earth rotation, the relative velocity of the satellite is approximated[36] as follows:

$$v_r = \sqrt{\frac{\mu(1+ecosE)}{a(1-ecosE)}} - \omega_E a\sqrt{1-e^2}cosi\sqrt{\frac{1-ecosE}{1+ecosE}}\ m/s \tag{3}$$

where ω_E is the Earth rotation rate, equal to $7.2722 * 10^{-5} rad/s$. From this calculation block, we find the minimum altitude where the atmospheric drag can be compensated by the thruster. For circular orbits, relative velocities of the spacecraft with respect to the atmosphere is given by

$$v_r = \sqrt{\frac{\mu_E}{a}} - \omega_E acosi\ m/s,$$

from (3). Then using (2), the deceleration can be derived as a function of altitude and inclination and compared with known values, such as a known initial on-orbit altitude of a CubeSat mission.

D. Deployment using J-SSOD from ISS

In the absence of firm mission definition details, for the remainder purposes of this preliminary analysis, the International Space Station (ISS) will be adopted as the launching point of a μCAT subsystem equipped CubeSat, via the J-SSOD. The initial deployment[37] will be at the ISS altitude (385-425 km) and inclination (i_{ISS} ~51.6 deg.). Bearing in mind there is a safety zone of 200m around the ISS, a "keepout zone", $r_{ko} = 210m$, will be accounted for, at which stage, the spacecraft will be separating from the station with $V_{s_{aft}}$ m/s in the direction of the *aft* vector, and $V_{s_{nadir}}$ m/s in the direction of the *nadir* vector, at an angle of θ_s degrees away from *nadir*, in the aft-nadir plane, with a total impulsive ΔV equal to the initial separation velocity, V_s m/s. $If\ \theta_s = 45^\circ, V_s = 1.1\ m/s$,

$$\begin{aligned} V_{s_{aft}} &= V_s * \cos(\theta_s)\ \ m/s \\ V_{s_{nadir}} &= V_s * \sin(\theta_s)\ m/s \end{aligned} \tag{4}$$

After the initial time t_{ko} required to drift slowly away from the ISS, past the "keepout" zone, μCAT operations may be started. If t_{aft} and t_{nadir} are the times required to pass through the imaginary spherical boundary of r_{ko},

$$t_{aft_{ko}} = \frac{r_{ko}}{V_{s_{aft}}}$$
$$t_{nadir_{ko}} = \frac{r_{ko}}{V_{s_{nadir}}} \tag{5}$$
$$t_{ko} = \lceil \max\left(t_{aft_{ko}}, t_{nadir_{ko}}\right) \rceil$$

Note, here a ~10 m margin of distance outwards from the official ISS keepout zone is employed. The ΔV impulsive maneuver in the aft direction can be utilized to calculate speed of the spacecraft on a Hohmann elliptical trajectory, referred to as Orbit #2, after it departs from the original ISS orbit, referred to as Orbit #3. The radial distance to the apogee of Orbit #2, jurst short of orbit #3 is at B, designated r_B, less the separation distance during the initial deployment period.

The semi-major axis can be calculated by the relationship of spacecraft velocity to the total mechanical energy of the orbit, taking into account the original velocity of the ISS, V_{ISS}, and its apogee $r_{a_{ISS}}$, perigee $r_{p_{ISS}}$, true anomaly averaged radius, $r_{\theta_{avg_{ISS}}}$ at time of deployment:

$$r_{a_{ISS}} = R_E + a_{ISS}\ (km)$$
$$r_{p_{ISS}} = R_E + p_{ISS}\ (km) \tag{6}$$
$$a_{ISS} = \frac{1}{2}\left(r_{a_{ISS}} + r_{p_{ISS}}\right)\ (km)$$

$$r_{\theta_{avg_{ISS}}} = \sqrt{\left(r_{p_{ISS}} r_{a_{ISS}}\right)}\ (km)$$
$$V_{ISS} = \sqrt{2\mu_E\left(\frac{1}{r_{\theta_{avg_{ISS}}}} - \frac{1}{2a_{ISS}}\right)}, when\ r = r_{\theta_{avg}} \tag{7}$$

Applying logic, we derive post-deployment spacecraft velocities and position.

$$s_{nadir_{ko}} = V_{s_{nadir}} t_{ko}\ \ (min.seperation)$$
$$\Delta V_B = V_{s_{aft}}\ (km/s)$$
$$V_{2_B} = V_{ISS} - \Delta V_B\ (km/s) \tag{8}$$
$$r_{B=} r_{a_{ISS}} - s_{nadir_{ko}} (km)$$

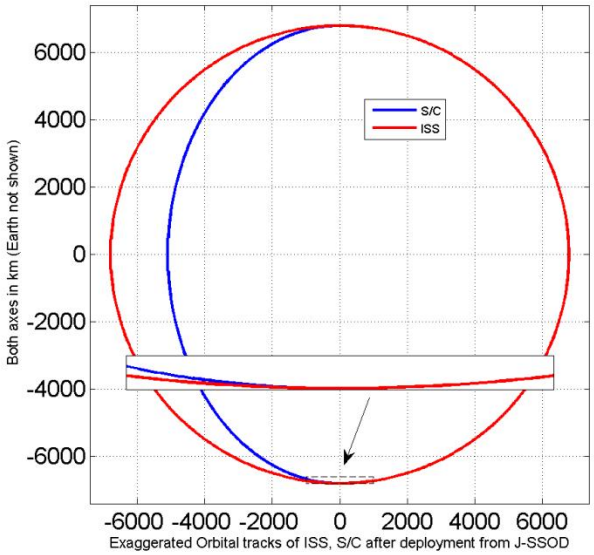

Figure 6 Hohmann transfer orbit after J-SSOD deployment of s/c

The total mechanical energyϵ of Orbit #2 is a constant, allowing us to calculate eccentricity, e, semi-major axis, a_2, radius of perigee, r_{p_2} and apogee, r_{a_2}, through equation set (9)

$$\begin{aligned} \epsilon_2 &= \frac{V_{2_B}^2}{2} - \frac{\mu_E}{r_B} \\ a_2 &= -\frac{\mu_E}{2\epsilon_2}\ (km) \\ r_{p_2} &= 2a_2 - r_B\ (km) \end{aligned} \tag{9}$$

$$\begin{aligned} r_{a_2} &= r_B\ (km) \\ e_{sc} &= \frac{r_{a_2} - r_{p_2}}{r_{a_2} + r_{p_2}} \end{aligned}$$

An exaggerated view of the orbital tracks of the ISS (red) and the spacecraft orbit (blue) after deployment from the J-SSOD is presented in FIGURE XX. It may be noticed that the semi-major axis of the transfer orbit is less than that of the ISS as it is a smaller energy orbit.

E. Orbit Circularization

Small errors in the initial orbit delivered by launch vehicle can be corrected by using the μCAT thruster subsystem. Here, we provide a simplified analysis for in-plane maneuvers to circularize the initial orbit with small corrections for semi-major axis.

Consider a fixed thrust u tangent to an orbit path. Low thrust spread over the entire orbit is inefficient and it requires large amount of propellant mass. To improve the overall efficiency, operation of low-thrust devices can be restricted to a part of an orbit. Here, perigee-centered burn and apogee-centered burn are defined by burn arcs α in terms of eccentric anomaly E as follows:

$$\begin{aligned} Perigee - centered\ burn\ (\sigma = -1): -\alpha \le E \le \alpha \\ Apogee - centered\ burn\ (\sigma = +1): \pi - \alpha \le E \le \pi + \alpha, \end{aligned} \tag{10}$$

where the binary parameter, σequals -1 for perigee burns, and +1 for apogee burns. The corresponding burn duration per revolution is given by:

$$t_{burn} = 2\sqrt{\frac{a^3}{\mu_E}}(\alpha + \sigma e sin\alpha) \tag{11}$$

Lagrange planetary equations describe variations of orbital elements due to perturbation. They are integrated over burn arcs to determine the change of orbital elements due to thruster per revolution, and they are divided by the orbital period to obtain the secular rates of change of orbital elements[29]. The rates of change for the semi-major axis and eccentricity are given by:

$$\frac{da}{dt} = \frac{2u_t}{\pi}\sqrt{\frac{a^3}{\mu_E}}\int_0^{\alpha}\sqrt{1 - e^2\cos^2 E}\,dE \tag{12}$$

$$\frac{de}{dt} = \frac{2u_t}{\pi}\sqrt{\frac{a}{\mu_E}}(1 - e^2)\int_0^{\alpha}\frac{cosE(1 - ecosE)}{\sqrt{1 - e^2\cos^2 E}}dE, (perigee\ burn: \sigma = -1) \tag{13}$$

$$\frac{de}{dt} = \frac{2u_t}{\pi}\sqrt{\frac{a}{\mu_E}}(1-e^2)\int_{\pi}^{\pi+\alpha}\frac{cosE(1-ecosE)}{\sqrt{1-e^2\cos^2 E}}dE, (apogee\ burn: \sigma = +1) \tag{14}$$

where u_t denotes the tangential acceleration due to the thrust. Note that $\frac{da}{dt}$ is identical for perigee burn and apogee burn. When $u_t > 0$ (acceleration), perigee burns increase eccentricity e, and apogee burns decrease e. These equations can be used for preliminary analysis for orbit circularizations. Suppose that the initial semi-major axis and the initial eccentricity are given by a_0 and $e_0$respectively. Let the desired semi-major axis and the eccentricity be $a_d$and $e_d$respectively. Diving (12) by (13) (or (14) for apogee burn), and assuming that the eccentricity is sufficiently small, we obtain:

$$\left(\frac{1}{a}\frac{da}{de} = -\frac{\sigma\alpha}{sin\alpha}\right) \approx \left(\frac{\frac{\Delta a}{a}}{\Delta e} = \frac{\frac{a_d}{(a_0-1)}}{-e_0}\right) \tag{15}$$

For a given a_d, a_0, e_0, we solve this equation for α to obtain the required burn arc for orbit circularization. The corresponding variations of a and e are computed by numerically integrating (12)-(14). The corresponding velocity change is described by:

$$\frac{dv}{dt} = \frac{\alpha u}{\pi} \tag{16}$$

from which the total velocity change is computed. The resulting consumption of mass propellant is given by:

$$m_p = m_0(1 - \exp\left(-\frac{\Delta v}{g_0 Isp}\right) \tag{17}$$

where the specific impulse is assumed to be constant, and in this application, 3100 seconds.

F. Inclination Correction

Once an orbit is circularized, the satellite can be re-oriented at 90to the flight path to generate thrust normal to the orbital plane. This can be used to correct the inclination errors induced by the launch vehicle. Similar to (12)-(14), when thrust is normal to the orbital plane, the secular rates of change of the inclination and the argument of perigeeω are given by:

$$\frac{di}{dt} = -\frac{u_n}{2\pi}\sqrt{\frac{a}{\mu_E}}cos\omega\frac{2\sigma sin\alpha(1+e^2)+3e\alpha+e\,cos\alpha\,sin\alpha}{\sqrt{1-e^2}}, \tag{18}$$

$$\frac{d\omega}{dt} = -\frac{u_n}{2\pi}\sqrt{\frac{a}{\mu_E}}cot\ i\cos\omega\frac{2\sigma sin\alpha(1+e^2)+3e\alpha+e\,cos\alpha\,sin\alpha}{\sqrt{1-e^2}} + A(a,e,i), \tag{19}$$

where $u_n$denotes the acceleration due to thruster, normal to the orbital plane, and $A(a,e,i)$ denotes the drift rates of ω due to J_2effects. When $e = 0$, the rate of change of i is simplified as:

$$\frac{di}{dt} = -\frac{u_n}{\pi}\sqrt{\frac{a}{\mu_E}}\sigma\cos\omega\sin\alpha \tag{20}$$

Note that the sign of $\frac{di}{dt}$is determined by $\sigma cos\omega$. To maximize $\frac{di}{dt}$, we assume that both of perigee-centered burn and apogee-centered burn occur on each revolution with $\alpha = 90^\circ$ (continuous burn), and the thrust direction is reversed according to the sign of $\sigma cos\omega$. Then we obtain:

$$\left|\frac{di}{dt}\right| = \frac{2u_n}{\pi}\sqrt{\frac{a}{\mu_E}}|\cos\omega| \tag{20}$$

Note this approach is most effective, when $\omega = 0^\circ \ or \ 180^\circ$, but at low earth orbits, it is difficult to keep ω near those values as it drifts due to the J_2 effects. These are numerically integrated to obtain the variation of i.

III. Use Case

A. Definition

The atmospheric density at common altitudes (100-900 km) was modeled using the MSISE-90 model which describes the neutral temperature and densities in Earth's atmosphere from ground to thermospheric heights. High/Mean/Low Solar activity was modeled. A spacecraft nominal mass size of 1.124 Kg was selected, assuming a simple 1U Cubesat with three thruster channels, or a 1U Cubesat with a single thruster and robust PPU. Selected altitude ranges (Table 1) were compared with the force that could be produced by μCAT subsystems operating per Table 2. Each impulse bit produced, on average, 1.15 μNs of thrust.

Table 1 Target Altitudes (Modeling/Simulation)

Target Altitudes (km)	Description
240	LEO orbit insertion and deployment of PhoneSat mission on Antares maiden flight[12, 21, 24, 25].
385	ISS altitude (low estimate[37])
425	ISS altitude (high estimate[37])

Table 2 Target uCAT Thruster Operating Levels (Modeling/Simulation)

Target Thruster Operating Levels	
Multiple Channels	Single Channel
2 Ch. 1 Hz	1 Ch, 1 Hz
2 Ch. 50 Hz	1 Ch. 50 Hz
3 Ch. 1 Hz	
3 Ch. 50 Hz	
50 Ch. 1 Hz (impractical)	

The position of the ISS on September 18, 2013 at 2243 EDT was obtained from SpaceTrack[6] information service. The values of the key orbital elements were as follows:

- Node: Zarya/ISS
- Apogee: 418 km
- Perigee: 414 km
- Period: 92.88 m
- Inclination: 51.65 degrees

A J-SSOD deployment of a hypothetical CubeSat was modeled using (4)-(9) assuming a deploy direction angle of 0 degrees, in the aft direction, with a separation velocity of 1.1 m/s. The keepout zone was artificially defined to be 210 km from the ISS center of mass, and it was assumed there were no protrusions/fuselage sections or other space objects in the exit cone of the departing spacecraft. No on-orbit thruster operations were modeled within the time the spacecraft remained in the keepout zone.

Assuming the spacecraft separated cleanly away from the ISS, orbit circularization was modeled using (10)-(17) and making assumptions about thruster operating levels (e.g., 10 Hz, 20 Hz, 30 Hz, 50 Hz for a single thruster channel) and varying separation ranges (e.g., min. 10 km, max. 90 km) between the semi-major axis magnitude of

[6] http://www.space-track.org (subscription required)

the initial and desired orbits. At the conclusion of the orbit circularization stage, further steps were taken to model an inclination correction maneuver using (18) – (20).

B. Results – Initial Orbit

It was seen that the density of the atmosphere falls rapidly with higher altitudes (**Figure 7**), and increase in solar activity produces the opposite effect. Utilizing markers to denote the altitudes of interest and considering only mean and high solar activity levels, it was seen that a 1 channel thruster spacecraft, operating at 1 Hz, would have to be operated at altitudes greater than 440.9 km in order to overcome drag. Additional channels (at 1 Hz) would decrease the minimum altitude required to operate (e.g., 400.4 km for 2 Ch, and 377.9 km for 3 Ch. operations) If a system could be designed that would accommodate the power and mass needs of 50 channel operation, at 1 Hz, it was seen that the resultant force could be used to overcome drag at a very low altitude (e.g, PhoneSat's 1st mission in April 2013) at 241.3 km. On the other hand, if 50 Hz were adopted as a typical operating mode for μCAT systems, then drag produced due to high levels of solar activity could be overcome in a much easier manner (Figure 8).

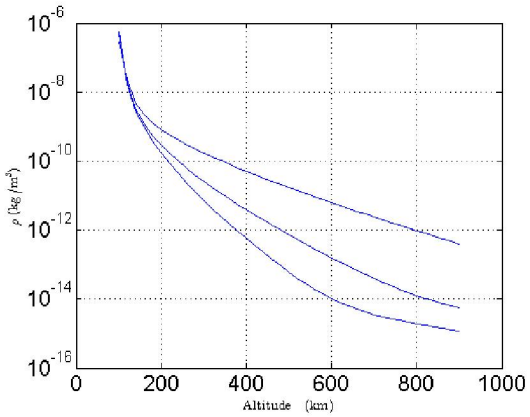

Figure 7 Atmospheric density variation, according to the MSIS90E model for three levels of solar activity[35]

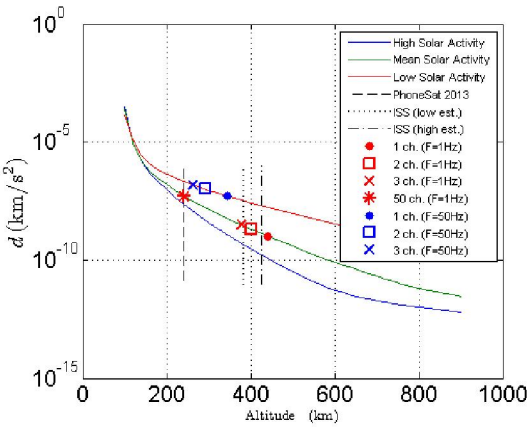

Figure 8 Deceleration due to atmospheric drag

C. Results – Deployment using J-SSOD from ISS

Values were obtained for the use case defined above:

- Ballistic Coefficient: 0.19573 (m^2/kg)
- Perigee Radius (ISS): 6792 (km)/Perigee Alt. 418 (km)
- Apogee Radius (ISS): 6796 (km)/Apogee Alt. 414 (km)
- Eccentricity : 0.00029438
- Semi-Major axis (ISS): 6794 (km)
- Period (ISS): 92.886 (mins.)
- Angular Momentum (ISS): 52039 (km^2/s)
- True Anomaly Averaged Radius: 6794 (km)
- Speed of ISS when r=r_theta_avg: 7.6596 (km/s)
- Total separation velocity: 1.1 (m/s)
- Aft separation velocity: 0.778 (m/s)
- Nadir separation velocity: 0.778 (m/s)
- Time to clear keepout zone: 270 (s)
- Velocity on Orbit #2 at B: 7.659 (km/s)
- Eccentricity: 6.04E-5
- Inclination: 0.9 (radians)
- Semi-Major Axis: 6796.20057 (km)
- Semi-Minor Axis: 6796.20055 (km)

D. Results – Orbit Circularization

Numerical results to circularize orbits (with a difference of 10-90 km between initial/desired altitudes, close to ISS altitude) are illustrated in Figure 9 and Figure 10. It is shown that the orbit can be circularized while correcting the semi-major axis by 26.41 km in 21.56 days, if the μCAT system is operated at 10 Hz. For higher operating frequencies, the required duration to circularize is smaller, such as only 12.51 days to overcome a difference of 90.41 km, utilizing μCAT systems being operated at 50 Hz. The corresponding propellant consumption has been calculated and in the first case, would have only required less than 0.25 gram, whereas the 50 Hz case would require close to 2 grams of propellant.

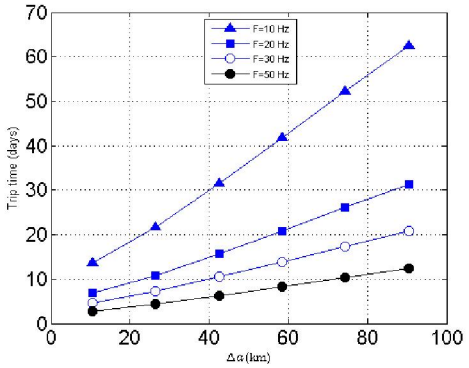

Figure 9 Circularization to desired orbit maneuver, for various pulse rates

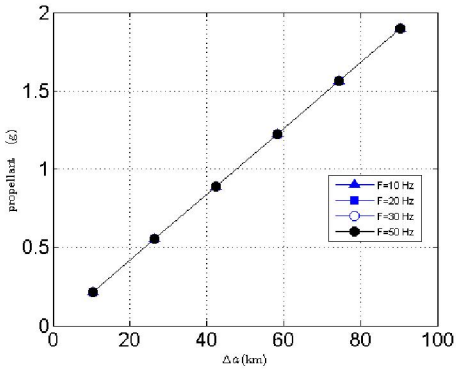

Figure 10 Propellant requirements for circularization maneuver

E. Results – Inclination

It can be seen in Figure 11, Figure 12, Figure 13that inclination maneuvers are more costly (more propellant, more time) required compared to orbit circularization. When thrust of 10 Hz is utilized, it will take 41 days to correct an inclination error of 0.1 degrees with a small amount of propellant (approx.. < 1.5 gms). If 50 Hz thrust levels could be utilized, then that period would be reduced to approximately 5 days, consuming about 0.7 gms.

IV. Conclusions

Preliminary orbital analyses are provided for a 1U Cubesat, with 1.124 Kg mass, and a μCAT "In-Space" propulsion subsystem, based on averaged Lagrange planetary equations. The following results have are obtained:

- μCAT subsystems able to perform between 1-50 Hz are recommended for initial space missions.
- Single channel thruster systems are capable of overcoming high solar activity induced drag in LEO, if used with higher pulse rates, or in arrays.
- The initial periapsis altitude should be greater than 300 km to cancel atmospheric drag for mean solar activity.
- The initial orbit delivered by launch vehicle can be circularized with semi-major axis correction. The semi-major axis can be changed by 27 km over 22 days.
- Inclination correction maneuvers require longer time period. It can be changed less than $\Delta i = 0.1^\circ$ per 5 days, at an operating rate of 50 Hz.

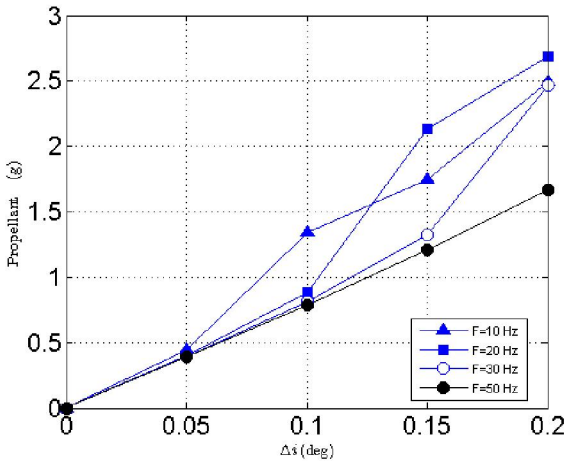

Figure 11 Inclination Correction Maneuver propellant usage

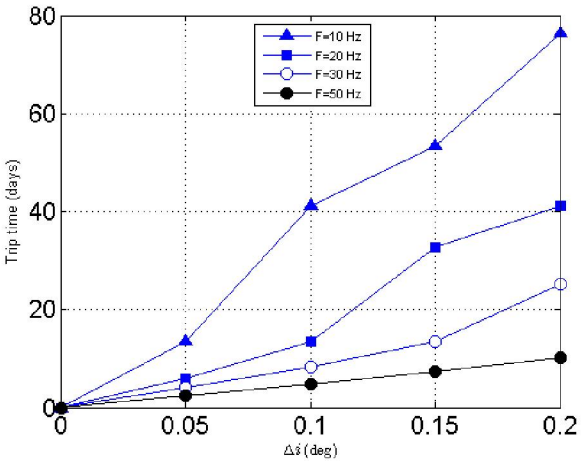

Figure 12 Trip time for inclination maneuver

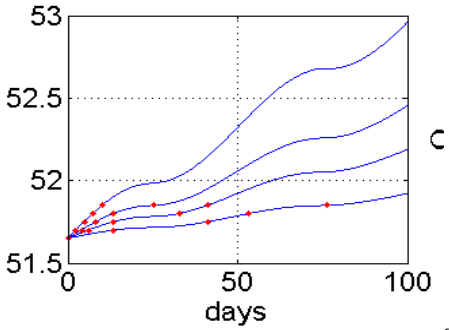

Figure 13 Variations in inclination for different thrust levels and transit times

References

[1]. Keidar, M., and Boyd, I., "Effect of a magnetic field on the plasma plume from Hall thrusters," *Journal of Applied Physics,* Vol. 86, No. 9, 1999, pp. 4786-4791. doi: 10.1063/1.371444

[2]. Keidar, M., Schein, J., Wilson, K., Gerhan, A., Au, M., Tang, B., Idzkowski, L., Krishnan, M., and Beilis, I. I., "Magnetically enhanced vacuum arc thruster," *Plasma Sources Science and Technology,* Vol. 14, 2005, pp. 661-669.

[3]. Zhuang, T., Shashurin, A., Brieda, L., and Keidar, M., "Development of Micro-Vacuum Arc Thruster with Extended Lifetime," *31st International Electric Propulsion Conference,* Vol. 2009, 2009,

[4]. Zhuang, T., Shashurin, A., Denz, T., Chicka, D., and Keidar, M., "Micro-Vacuum Arc Thruster with Extended Lifetime," *45th AIAA/ASME/SAE/ASEE Joint Propulsion Conference & Exhibit,* Denver, CO, 2009,

[5]. Zhuang, T., Shashurin, A., Haque, S., and Keidar, M., "Performance characterization of the micro-Cathode Arc Thruster and propulsion system for space applications," *46th AIAA/ASME/SAE/ASEE Joint Propulsion Conference & Exhibit,* Nashville, TN, 2010, pp. 8.

[6]. Zhuang, T., Shashurin, A., Teel, G., Chiu, D., and Keidar, M., "Co-axial Micro-Cathode Arc thruster (CA-uCAT)
Performance Characterization," *47th AIAA/ASME/SAE/ASEE Joint Propulsion Conference & Exhibit,* 2011,

[7]. Vail, P., Pancotti, A., Zhuang, T., Shashurin, A., Keidar, M., and Denz, T., "Performance Characterization of Micro-Cathode Arc Thruster (uCAT)," *47th AIAA/ASME/SAE/ASEE Joint Propulsion Conference & Exhibit,* 2011,

[8]. Taisen Zhuang, Shashurin, A., and Keidar, M., "Microcathode Thruster (\mu\hbox) Plume Characterization," *IEEE Transactions on Plasma Science,* Vol. 39, No. 11, 2011, pp. 2936-2937. doi: 10.1109/TPS.2011.2160407

[9]. Zhuang, T., Shashurin, A., Keidar, M., and Beilis, I., "Circular periodic motion of plasma produced by a small-scale vacuum arc," *PLASMA SOURCES SCIENCE & TECHNOLOGY,* Vol. 20, No. 1, 2011,

[10]. Zhuang, T., Shashurin, A., Beilis, I., and Keidar, M., "Ion velocities in a micro-cathode arc thruster," *Physics of Plasmas,* Vol. 19, No. 6, 2012, pp. 063501-063501-5. doi: 10.1063/1.4725500

[11]. Denz, T. A., "Performance Evaluation of a Magnetically Enhanced Micro-Cathode Vacuum Arc Thruster," 2012,
[12]. Haque, S. E., Tintore, O., Uribe, E., Agasid, E., and Keidar, M., "Micro-Cathode Arc Thruster PhoneSat Experiment for Small Satellites," *International Electric Propulsion Conference,* Washington, DC, 2013,
[13]. Woellert, K., Ehrenfreund, P., Ricco, A. J., and Hertzfeld, H., "Cubesats: Cost-effective science and technology platforms for emerging and developing nations," *Advances in Space Research,* Vol. 47, No. 4, 2011, pp. 663-684. doi: 10.1016/j.asr.2010.10.009
[14]. VanOutryve, C. B., "A thermal analysis and design tool for small spacecraft," 2008,
[15]. Diaz-Aguado, M. F., Ghassemieh, S., Van Outryve, C., Beasley, C., and Schooley, A., "Small Class-D spacecraft thermal design, test and analysis - PharmaSat biological experiment," 2009, pp. 1-9.
[16]. Bramall, N., Ricco, A., Squires, D., Santos, O., Friedericks, C., Landis, D., Jones, N., Salama, F., Allamandola, L., Hoffmann, S., Quinn, R., Mattioda, A., Bryson, K., Chittenden, J., Cook, A., Taylor, C., Minelli, G., and Ehrenfreund, P., "The development of the Space Environment Viability of Organics (SEVO) experiment aboard the Organism/Organic Exposure to Orbital Stresses (O/OREOS) satellite," *Planetary and Space Science,* Vol. 60, No. 1, 2012, pp. 121-130. doi: 10.1016/j.pss.2011.06.014
[17]. Jacob Ward, "A New Standard," *Popular Science,* Vol. 280, No. 2, 2012, pp. 23.
[18]. Mahoney, J., "Everyman's satellite: NASA PhoneSat.(BEST OF WHAT'S NEW: AEROSPACE)," *Popular Science,* Vol. 281, No. 6, 2012, pp. 55.
[19]. Anonymous "HTC and NASA to send Nexus One into space in 2013 as part of PhoneSat program," *Engadget Mobile [Engadget Mobile - BLOG],* 2012,
[20]. Anonymous "NASA and Ham Radio Operators Piece Together the PhoneSat Picture," Federal Information & News Dispatch, Inc, Lanham, 2013.
[21]. Linda Bell, "NASA Completes Successful PhoneSat Mission," *NASA Tech Briefs,* Vol. 37, No. 7, 2013, pp. 8.
[22]. Michael Cooney, "NASA smartphone satellites beam clear images of Earth: NASA's PhoneSats were an experiment to develop super-cheap satellites," *Network World (Online),* 2013,
[23]. Anonymous "NASA'S PhoneSat Gets the Science Best of What's New Award," *Entertainment Close - Up,* 2012,
[24]. Anonymous "NASA'S PhoneSat Wins the Science Best of What's New Award," *Wireless News,* 2012,
[25]. Mark K. Matthews, "NASA's tiny 'PhoneSats' from smartphones show promise," *McClatchy - Tribune Business News,* 2013,
[26]. Anonymous "NASA Announces New CubeSat Space Mission Candidates," *Targeted News Service,* 2013,
[27]. Anonymous "NASA Announces Fourth Round of CubeSat Space Mission Candidates," Federal Information & News Dispatch, Inc, Lanham, 2013.
[28]. Anonymous "NASA Announces Candidates for Cubesat Space Missions," Federal Information & News Dispatch, Inc, Lanham, 2011.
[29]. Pollard, J., *Simplified Analysis of Low-Thrust Orbital Maneuvers,* 2000,
[30]. Pollard, J. E., "Simplified Approach for Assessment of Low-Thrust Elliptical Orbit Transfers," *25th International Electric Propulsion Conference, Cleveland, OH,* 1997, pp. 97-160.
[31]. Danby, J. M. A., "Fundamentals of celestial mechanics," 1988,
[32]. Anonymous "Asia Pacific News," *Via Satellite,* Vol. 28, No. 2, 2013,
[33]. Jessica Nimon for ISS Science News, "The New and Improved ISS Facilities Brochure," *UPI Space Daily,* 2013,
[34]. Rebecca Lincks, "JAXA Introduces New CubeSat LauncherReb," *Satellite Today,* Vol. 11, No. 251, 2012,
[35]. HEDIN, A., "EXTENSION OF THE MSIS THERMOSPHERE MODEL INTO THE MIDDLE AND LOWER ATMOSPHERE," *JOURNAL OF GEOPHYSICAL RESEARCH-SPACE PHYSICS,* Vol. 96, No. A2, 1991, pp. 1159-1172.
[36]. Belcher, S., Rowell, L. N., and Smith, M., "Satellite Lifetime Program," 1964,
[37]. Pournelle, R., "Small Satellite Deployment from ISS," 2013,